

MODELING OF AIR FLOW OVER A GENERIC AIRCRAFT CARRIER WITH AND WITHOUT ISLAND STRUCTURE

(Reference No: IJME686, DOI No: 10.5750/ijme.v163iA3.803)

MP Mathew¹, SN Singh¹, SS Sinha¹ and R Vijayakumar²

¹Department of Applied Mechanics, Indian Institute of Technology Delhi, New Delhi, India

²Department of Ocean Engineering, Indian Institute of Technology Madras, Chennai, India.

KEY DATES: Submitted: 30/11/20; Final acceptance: 12/08/21; Published 16/11/21

SUMMARY

The study of external aerodynamics of an aircraft carrier is of utmost importance in ensuring the safety of aircraft and pilots during take-off and recovery. The velocity deficit in the forward direction and the downwash together combine to give a sinking effect to the aircraft, along its glideslope path and is known as the ‘burble’ in naval aviation parlance. This phenomenon is primarily responsible for the potential increase in pilot workload on approach to the aircraft carrier. There is little literature in the open domain regarding ways and means to alleviate the burble effect. Unlike in the case of the automobile industry, which has the generic ‘Ahmed body’ and for the frigates/destroyers, for which there is the Simplified Frigate Ship (SFS), on which experiments and validation through CFD could be carried out, by researchers from all over the world, there is no generic Aircraft Carrier model for carrying out experiments and validation of CFD codes. The aim of this study is to define the Generic Aircraft Carrier Model (GAC), as developed at IIT Delhi, and to carry out numerical studies on the GAC and a variant of GAC without the island, BGAC (Baseline GAC), to assess the contribution of the island to the burble behind an Aircraft Carrier. This study gives a quantitative estimation of the effect and contribution of individual components of an Aircraft Carrier (like flight deck, island, etc.) to the burble behind the carrier, and would give a Naval Ship Designer an understanding of the effect of the geometrical configuration of the flight deck and the island on generation of the burble behind the carrier, which could aid the designer in potentially reducing the pilot workload.

NOMENCLATURE

BGAC	Baseline Generic Aircraft Carrier
C_p	Pressure Coefficient
CFD	Computational Fluid Dynamics
CVA	Attack Aircraft Carrier
CVG	Columnar Vortex Generator
CVN	Nuclear Aircraft Carrier
GAC	Generic Aircraft Carrier
HPC	High Performance Computing
L	Length of Ship model (m)
LDV	Laser Doppler Velocimetry
LHD	Landing Helicopter Dock
MILES	Monotone Integrated Large Eddy Simulation
NAEL	Naval Air Engineering Laboratory
NAVAIR	Naval Air Systems Command
NSWC	Naval Surface Warfare Center
p_∞	Free stream reference pressure ($N\ m^{-2}$)
p_i	Local pressure at i^{th} location ($N\ m^{-2}$)
PIV	Particle Image Velocimetry
RANS	Reynolds Averaged Navier Stokes Equation
SRVL	Shipborne Rolling Vertical Landing
k & TKE	Turbulence Kinetic Energy
$TKE_{Average}$	Average Turbulence Kinetic Energy (J/Kg)
V	Free stream velocity ($m\ s^{-1}$)
u	Mean velocity in x -direction ($m\ s^{-1}$)
$u_{Av_variation}$	Average variation in u -velocity (m/s)
w	Mean velocity in z -direction ($m\ s^{-1}$)
$w_{Av_variation}$	Average variation in w -velocity (m/s)

x	Distance from ship’s bow (m)
ρ	Density of fluid ($kg\ m^{-3}$)

1. INTRODUCTION

For any pilot, the task of landing an aircraft on to an aircraft carrier would be the most challenging. The pilot has to, not only land the aircraft on a moving ship, but he/she would also have to cope with a new challenge, the burble along the glideslope path, which is not encountered, in the case of land based aircraft. Unlike a land based airfield, the island superstructure, flight deck and the hull of an aircraft carrier would generate a turbulent airflow aft of the ship characterized by regions of large separated flows (K Vignesh Kumar *et al.*, 2018). This region of disturbed air flow has come to be known as the burble, and it is often encountered by pilots immediately prior to landing (Cherry and Constantino, 2010). This burble, which is manifested as reduced wind velocity and a downwash causes the aircraft to drop momentarily, primarily because of decrease of lift force on the wings of the aircraft (Cherry and Constantino, 2010). This has to be stabilised by a momentary thrust in the upward direction, so that glideslope path for aircraft can be maintained. Further, the motions of the flight deck in high seas like roll and pitch add on to the “burble effect”. The burble effect has been reported by pilots to occur within the final half mile (typically about 2.5 times the length of the carrier) aft of the touch down point (Cherry and Constantino, 2010). This ‘burble effect’ could be perilous to the pilot because the pilot clears the ramp of

an aircraft carrier by a margin of only 3-4 m with the touch down 1 sec later. As the aircraft approaches the ramp of the carrier, usually at a glideslope angle between 3 to 4 degrees, any change in the vertical height of the aircraft over the ramp, because of the burble effect, would change the touchdown point by a ratio of 15:1. Further the situation could be aggravated because of ship motions, poor weather, strong winds and turbulence. The pilot encounters the burble during the last few seconds prior to touchdown, and the pilot normally has 1 to 2 sec after emergence from the disturbance, to decide whether to land or abort. The very act of taking such quick decisions, could increase the stress on the pilot and more so, when they know that a wrong decision on their part could have very serious consequences. This adds to the pilot's already stressed workload. As per a 1964 report for the US Navy, it was seen that, approximately 80% of all landing accidents and 25% of all landing attempts which result in either bolters or wave offs in the US Navy (which incidentally operates the largest number of Aircraft Carriers) can be attributed to inadequate vertical control (Durand and Teper, 1964). Between 1949 and 1988, the US Navy lost almost 12000 airplanes and over 8500 aircrew of all types (Smith, 2010). Though a majority of the accidents could be attributed to causes other than the "burble effect", we cannot overlook the fact that the "burble" does put considerable stress and adds on to the pilot's workload.

2. MOTIVATION FOR THE STUDY

Naval aviation pilots, are key personnel, who will ensure that the operational task for which the Carrier is deployed, is a success or a failure, be it in peace or wartime. Any changes to the design of an aircraft carrier, which would make the landing of an aircraft, as safe as possible, could potentially increase the operability of aircraft carriers even in dynamic sea conditions. A reduction in the burble effect / airwake wake turbulence behind an aircraft carrier, could potentially reduce the pilot stress and workload. A reduction in the turbulence behind an aircraft carrier, would require a thorough understanding of the external aerodynamics especially aft of an aircraft carrier along the approach path.

The primary motivation of this study is to carry out a survey of the studies that have been carried out in this field, and based on the gaps, the aim is to come up with a methodology for quantifying the burble effect and then using this mathematical construct, to analyse the aerodynamics behind a generic aircraft carrier with and without the island structure. From both the studies, the contribution of the island to the burble will be quantified.

3. REVIEW OF RELEVANT LITERATURE

An extensive literature survey focussing on the external aerodynamics of an aircraft carrier has been carried out. However, it is pertinent to mention, that since this field is related to naval operations especially that of aircraft

carriers, majority of the research that has taken place, is classified and hence not available in the open source. The literature survey is carried out under the following heads:

- (i) Early studies on flow over an aircraft carrier (up to early 1970s)
- (ii) Aircraft Carrier airwake studies: Experimental & Numerical.

The reasons for the period based classification of literature survey is because, prior to the 1970s, computational technology especially the hardware, was not very advanced. Computational Fluid Dynamics (CFD) was still in a very nascent stage, and the theoretical studies were carried out, based on the analytical work being done on the boundary layer effects on flat plates. The experimental instrumentation being used was also outdated, but rugged and time tested like pressure probes and anemometry for measuring velocity and pressure fields and smoke for the purposes of visualization in wind tunnels. Further, to check the reliability of the wind tunnel studies, full scale studies on aircraft carriers using instrumented aircraft were used. Post 1970s, advances in the field of experimental instrumentation, like the introduction of Laser Doppler Velocimetry (LDV) and Particle Image Velocimetry (PIV), brought a paradigm change in the way flow parameters including turbulence parameters can be measured. Further, the advent of High Performance Computing (HPC) and CFD, have revolutionized the field of aerodynamics, and it would not be long before its effect would be felt in the study of ship aerodynamics too.

3.1 EARLY EXPERIMENTAL STUDIES OF FLOW OVER AN AIRCRAFT CARRIER

One of the earliest studies on aircraft carriers was by Ringleb (Ringleb, 1963) who studied the causes of strong turbulence in the flow over an aircraft carrier and, in particular, near the landing area of aircraft, using the three dimensional smoke tunnel of the NAEL (Naval Air Engineering Laboratory) Philadelphia, Pennsylvania, on 3 models of aircraft carriers, then existing in the US Navy. His studies showed that it was not only the island, but the total body of the ship that contributed to the disturbed flow in the stern area. In his studies he brought out, that sharp edges on the above water surfaces of the ship and especially at the deck should be avoided.

Barnett and White (Barnett and White, 1963), compared experimentally the characteristics of external aerodynamics of various US Aircraft carriers to understand the relationship if any, between the geometrical features of an Aircraft Carrier and its airwake. A large number of full scale trials and model scale tests were conducted to map the airwake patterns around various Aircraft Carriers. They found good correlation between the various geometrical features of a carrier and its superstructure to the generated airwake. However, predicting the air wake characteristics of one carrier from the airwake characteristics of a different carrier with different geometrical features was not very successful.

Lehman (Lehman, 1966), undertook investigations in a water tunnel to obtain greater visual clarity of the turbulence generated by an aircraft carrier behind it. The study qualitatively found out that the notches on the flight deck and the superstructure were the two main sources for the flow disturbances. However, the complete elimination of the island only reduced the downstream disturbed flow marginally. The canted deck was one of the major contributors to downstream disturbances. Pitch motions produce greater turbulent disturbances compared to heave motions. Lehman's study was one of those rare studies, experimentally or otherwise, which considered the effect of ship motions on the airflow disturbances and one of the few experimental studies to be conducted in a water tunnel.

Fraundorf (Fraundorf, 1966), investigated various mechanisms (by carrying out a number of ship modifications), for reducing the airwake turbulence behind the carrier for ease in recovery of aircraft, by carrying out wind tunnel experiments using models of CVA(N) 19, CVA 41, CVA 62, and CVA 65 carriers.

Frost (Frost, 1968), applied the existing knowledge of the boundary layer theory over a flat plate, to the flow over an aircraft carrier and was able to show that an aircraft, even at a distance of 500 feet away from the touch down point would be in the vicinity of wake generated by boundary layer of the flight deck.

3.2 AIRCRAFT CARRIER STUDIES: EXPERIMENTAL & NUMERICAL

Researchers from the US Naval Air Systems Command (NAVAIR) were the pioneers in using CFD techniques to simulate the external aerodynamics of an aircraft carrier. All their CFD studies are carried out using CFD solver COBOLT with Monotone Integrated Large Eddy Simulation. One of their first studies (Polsky and Bruner, 2002) was to compute unsteady CFD simulations of a LHA-Class ship, which is akin to an aircraft carrier and results showed good comparison with test data from experiments. Thereafter on the same lines they went on to model the airwake for a simplified aircraft carrier model of CVN-73 (Polsky and Naylor, 2005). Wind tunnel data from NSWC Carderock, along the glideslope path was used for comparison with full scale CFD results and the comparisons with u and w components of velocity were good. CFD calculations were carried out with the Aft End cut-out region filled (See Figure 1). Although the velocity profiles did not significantly change, the flow field in the vicinity of the stern region showed substantial changes.

Effect of passive flow devices, especially bow flaps and Columnar Vortex Generators (CVG) on improving the airflow in the vicinity of an aircraft carrier, especially in the bow region have been studied experimentally (Landman *et al.*, 2005) as well as numerically (Czerwiec and Polsky, 2004). The studies

concluded that these devices reduced the turbulence and the flow separation region.

Countries other than USA, have Aircraft Carriers that have the ski-jump system, which consists of a parabolic/ angled ramp, which would give an angle of attack to the aircraft during take-off with corresponding increase in lift force, such that the aircraft can take off with lesser length of runway. The geometrical configuration of the ski-jump because of its sharp features could adversely impact the flow field in the vicinity of the bow region. The relative wind velocity is reduced because of the formation of the recirculation bubble in the bow region, with consequent reduction in aerodynamic lift. Bardera-Mora and his group from Madrid, Spain have been carrying out various wind tunnel tests using particle image velocimetry (PIV) on a model of aircraft carrier to reduce the turbulence levels in the bow region by using flaps and CVGs (Bardera-Mora *et al.*, 2016) (Bardera-Mora, Rodríguez-Sevillano, *et al.*, 2018). Their studies have shown that maximum reduction in the recirculation bubble, up to 50 %, was obtained with the CVG device (Bardera-Mora, Rodríguez-Sevillano, *et al.*, 2018). They have also studied the effect of cross wind on the landing spots of helicopters for an aircraft carrier (Bardera-Mora, León Calero, *et al.*, 2018), using wind tunnel experiments with laser Doppler anemometry and PIV techniques. The wind tunnel results have also been compared with full scale measurements on board, using Power Spectral Density Plots with reasonable agreement between both.

The minute details of hull appendages, masts and superstructure would make the geometry of an aircraft carrier extremely complex. The computational expense for carrying out CFD simulations including the time taken for meshing is dependent on the level of complexity of the geometrical model. Shipman *et al.* (Shipman *et al.*, 2005), investigated the accuracy and sensitivity of the airwake solution of an Aircraft Carrier Nuclear (CVN) with respect to several modelling parameters, like geometrical complexity and the level of resolution of boundary layers by comparing CFD results that they had obtained with the experimental data. The models used were CVN-76 with simple geometry superstructure and complex geometry superstructure. The results showed that a majority of the flow field was characterized by bluff body shedding from the larger entities that constitute an aircraft carrier.

Cherry and Constantino (Cherry and Constantino, 2010), carried out an experimental study on superstructure and flight deck effects on Carrier airwake. They carried out their experiments on a 6ft model of a simplified Nimitz class aircraft carrier, using a five-hole Pitot probe rake system. They conducted their experiments on two variants of an aircraft carrier, one fitted with the original box type Nimitz superstructure (SS) and the other fitted with Ford class superstructure, which was smaller and further aft and outboard from the centreline as compared to Nimitz SS. Velocity fields at a distance of one-third the length of the carrier aft of stern were mapped. Their studies showed that

the Ford SS generated lesser forward velocity deficit compared to the Nimitz SS model, primarily because of its smaller size. The second set of experiments were carried out to investigate the effect of filleting the notches of the Flight deck. Though the vortex and burble appeared relatively intact, the addition of the fillet drastically reduced the intensity of the deck/hull vortex.

One of the rare studies on the coupling effect between the aircraft and ship airwake was carried out by Shipman *et al.* (Shipman *et al.*, 2008) who investigated the coupling effects between an F/A-18 and CVN class aircraft carrier during its recovery to the flight deck using CFD solver CRUNCH CFD®. The mesh around the aircraft was dynamic. Their study demonstrated that there were differences between a standalone airwake and a coupled airwake and for integrating a ship airwake to flight simulators, it was prudent to consider coupling effects.

Researchers from the Flight Science & Technology (FS&T) research group at the University of Liverpool (UoL), have been in the forefront of carrying out successful CFD studies on Royal Navy frigates and destroyers for the past many years, for the purpose of piloted flight simulation. Currently, the FS&T group at UoL is working with BAE Systems to simulate high fidelity external aerodynamics on the Queen Elizabeth Class (QEC) carrier which could be integrated with the flight simulator operated by BAE Systems for training of pilots. Kelly, *et al.*, (Kelly, M. White, *et al.*, 2016), have simulated a high fidelity unsteady airwake field in the vicinity of the ship, using the commercially available CFD solver Ansys, employing the Delayed Detached Eddy Simulation (DDES) SST $k-\omega$ based turbulence model with third order accuracy. The CFD model was validated with the MILSPEC burble for 3° glideslope and experimental results using a 1:202 scale model of the QEC in the 90,000 litre recirculating water tunnel located at the University of Liverpool (Kelly, M. D. White, *et al.*, 2016) (Watson *et al.*, 2019). The comparison of the CFD simulation data with the experimental results for SRVL 7° centerline parallel approach showed very good agreement for u-component and v-component of the velocities.

In summary, the literature survey has identified an aircraft carrier airwake characteristics as a major operational challenge for understanding the carrier aircraft dynamic interface. Aerodynamic studies have been carried out on particular class of Aircraft Carriers like Nimitz Class (Cherry and Constantino, 2010) & LHD (Czerwiec and Polsky, 2004) by US Researchers, Queen Elizabeth Class by UK Researchers (Kelly, M. White, *et al.*, 2016) (Kelly, M. D. White, *et al.*, 2016) (Watson *et al.*, 2019), with an intention of providing airwake data to the flight simulators for training of pilots, but with no general guidelines for Naval Ship designers. There have been studies on improving the flow in the Bow region of an aircraft carrier with passive devices like CVGs, Bow Flaps, cylindrical section, etc. (Nangia and Lumsden, 2004; Landman *et al.*, 2005; Bardera-Mora *et al.*, 2016; Bardera-Mora,

Rodríguez-Sevillano, *et al.*, 2018). Studies have also been carried out to map the airwake around the flight deck regions, especially with a view point of optimizing the location of rotary aircraft landing points (Watson *et al.*, 2019). Studies have also confirmed, that modelling of intricate details of the flight deck and the island, may not be a necessity for capturing the global picture of the effect of the aircraft carrier airwake (Shipman *et al.*, 2005) (especially the burble effect along the various glideslope paths of fixed wing aircraft), especially aft of the stern, though for locations in the flight deck, such details might be required.

There has not been much work on the individual quantification of the turbulent airwake behind an aircraft carrier because of hull, flight deck and the superstructure. Further, there is a lack of literature especially in the open domain regarding the optimization of the island structure, with regards to reduction of the burble effect, aft of the stern of the superstructure. There have been no systematic studies conducted on the effect of design changes in the flight deck and island configuration and its effect on the flight qualities along specified glideslope paths. Further, unlike in the case of non-aviation ships like frigates and destroyers, for which there exists generic models, namely the SFS, SFS2 and NATO-GD (NATO Generic Destroyer) (Owen *et al.*, 2021), which could be used for generating experimental data for validation of CFD codes, there are no generic variant for the Aircraft Carriers. Individual researchers, carry out the experimental and CFD validation on aircraft carriers of their individual choice, which might give useful input for that particular class of aircraft carriers, but would not give a Naval Ship Designer any inputs for optimizing the various design parameters for a futuristic class of aircraft carriers.

4. PROPOSED GENERIC AIRCRAFT CARRIER

As brought out in the summary of the literature review, one of the drawbacks in conducting research on external aerodynamics of an aircraft carrier is the absence of a simplified version of an Aircraft carrier akin to the SFS in the case of frigates. To overcome this lacuna, a model of a Generic Aircraft Carrier (GAC) was developed (K Vignesh Kumar *et al.*, 2018), for a single island angled flight deck aircraft carriers. The model has the following salient features which are characteristic of aircraft carriers:-

- Asymmetry of the flight deck about centre line.
- Angled landing strip for simultaneous launch and recovery.
- Flared above water portion of the hull. The flight deck beam should be much wider than the beam at the water line. Large overhangs of deck with thick sponsons attached.
- Sharp edges and 'notches' on the flight deck.
- Island superstructure typically about 2-3% of gross volume of ship, placed aft of midship, along the starboard side.

Based on the above characteristics, a Generic Aircraft Model has been arrived at as shown in **Figure 1**. The figure shows a 1: 300 scaled model. The island superstructure has been modelled as a cuboid structure, as Shipman, et al., (Shipman *et al.*, 2005) have shown that the “airwake flow features are characterized by bluff body vortex shedding from larger geometric entities that comprise the ship geometry and the majority of the flow field, was not sensitive to the finer details of the island shape”.

5.1 GOVERNING EQUATIONS AND CHOOSING OF TURBULENCE MODEL

The numerical simulations were carried out by solving the Reynolds-averaged Navier-Stokes (RANS) equations by using the commercial CFD software ANSYS Fluent. The RANS equations are given below.

$$\frac{\partial \rho}{\partial t} + \frac{\partial}{\partial x_i} (\rho \bar{u}_i) = 0 \tag{1}$$

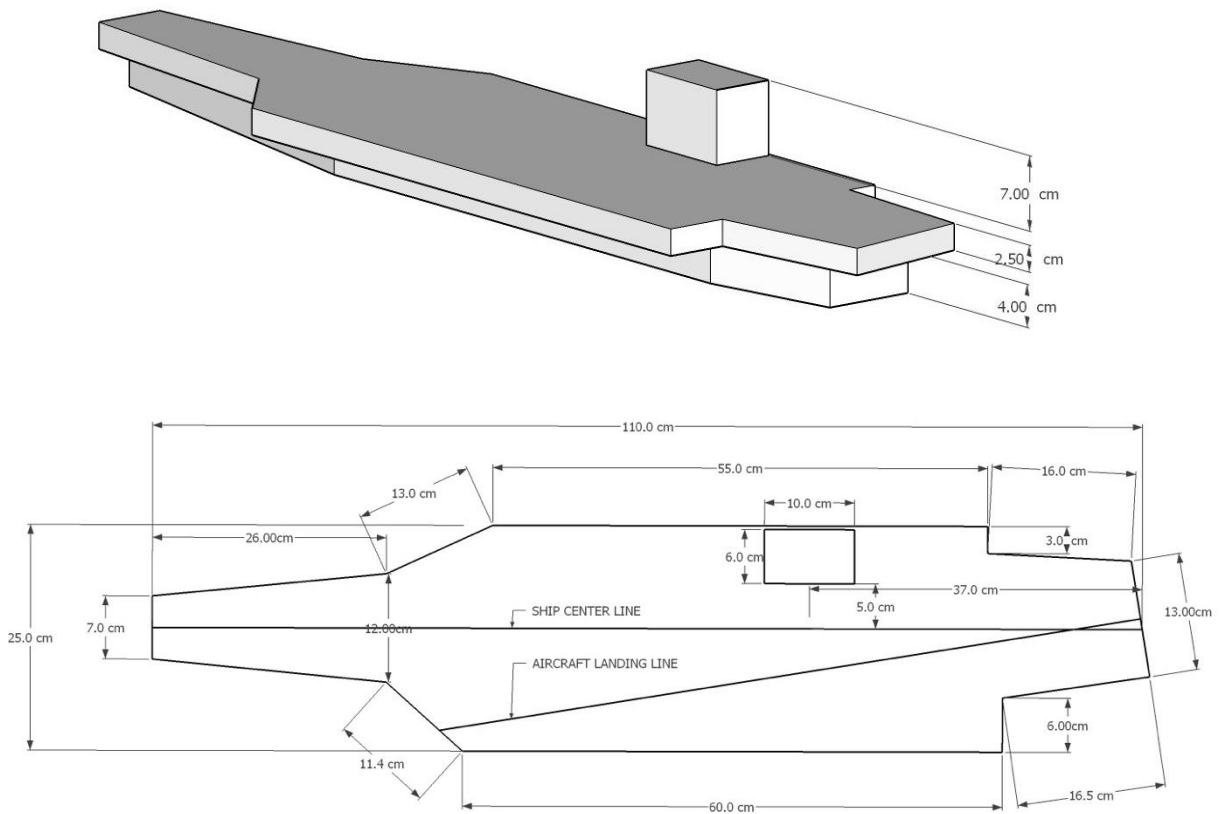


Figure 1: Dimensions of GAC

5. MATHEMATICAL FORMULATION OF THE AIR FLOW ISSUE

The aim of this particular study was to numerically simulate the airwake flow behind the Generic Aircraft Carrier and to quantify the turbulence because of the island alone. To do this, a variant of the GAC, without the island structure was also developed, which would henceforth be referred to as the Baseline GAC (BGAC). The GAC & BGAC models are shown in **Figure 2**. A comparative analysis of the airwake flow behind the GAC and BGAC configurations, would give an estimate of the turbulence caused by the island alone.

$$\frac{\partial}{\partial t} (\rho \bar{u}_i) + \frac{\partial}{\partial x_j} (\rho \bar{u}_i \bar{u}_j) = - \frac{\partial p}{\partial x_i} + \frac{\partial}{\partial x_i} \left[\mu \left(\frac{\partial \bar{u}_i}{\partial x_j} + \frac{\partial \bar{u}_j}{\partial x_i} - \frac{2}{3} \delta_{ij} \frac{\partial \bar{u}_k}{\partial x_k} \right) \right] + \partial / \partial x_j (-\rho \overline{u'_i u'_j}) \tag{2}$$

Several turbulence models are available which can be used to close the RANS equations, ranging from simple zero-equation model, to the most complex Reynolds stress transport models. From both, the physics of the problem, as well as validation through in-house data obtained experimentally using the GAC model and published experimental data (which would be covered in later sections), the most apt turbulence model for modelling the airwake around a generic aircraft carrier is the k- ω SST model (Menter, 1994). In the case of an aircraft

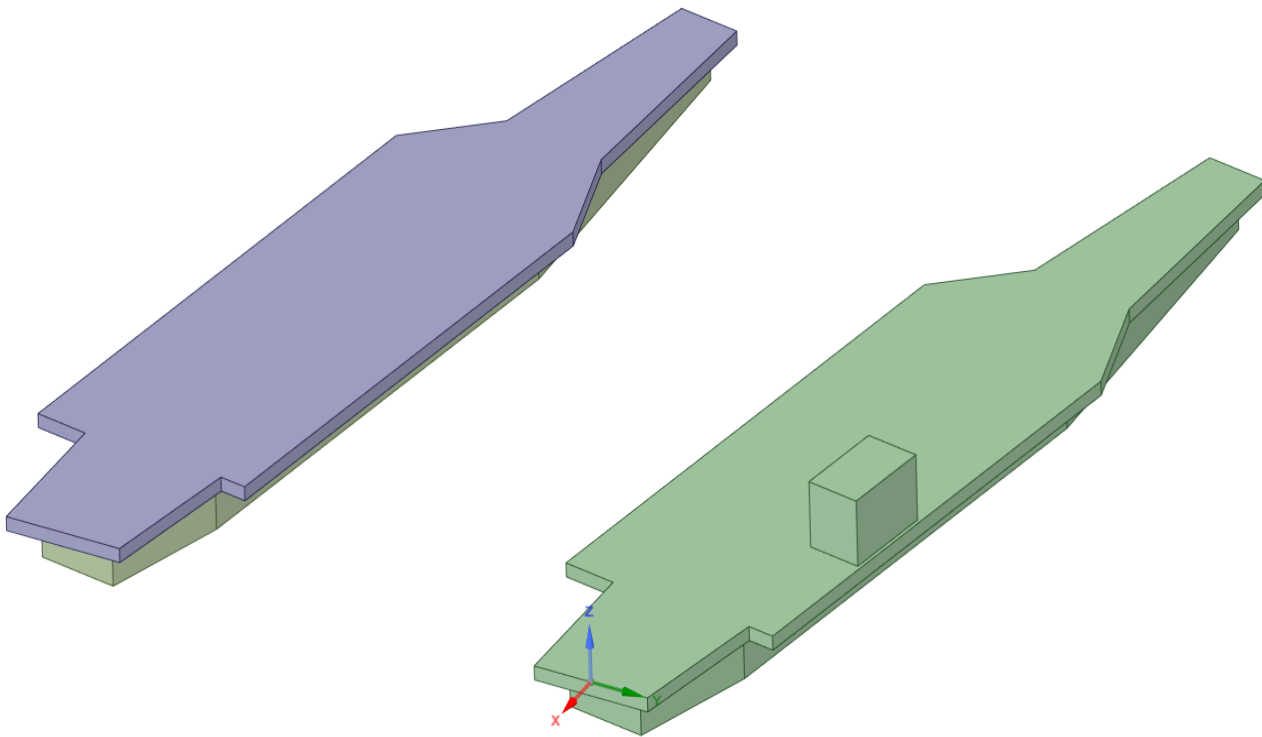


Figure 2: BGAC & GAC configurations

carrier, where the flight deck is essentially a flat plate, the effect of boundary layer growth could have a greater impact upon airwake over the landing spots, unlike that of a bluff bodied frigate or a destroyer, where airflow separates from the sharp edges on the superstructure and accuracy of capturing wall boundary layers is not important. Thus, in the case of an aircraft carrier, near wall boundary layer effects are as important as flow over a bluff-bodied island structure, and the turbulence model should be able to take into account, both the effects. Thus, from physics of the problem, the **k- ω SST** turbulence model which is a blend between k- ϵ and k- ω seems to be the most appropriate model.

5.2 SOLUTION STRATEGY

A summary of the Solver Options and Boundary Conditions, which have been used for the present study are tabulated in **Table 1** & **Table 2** respectively.

Table 1: Summary of Solution Options

Solver	Pressure Based
Pressure-Velocity Coupling	Coupled Solver with Pseudo Transient under-relaxation
Gradient Discretization (Convective & Diffusive terms)	Least Squares Cell Based
Pressure Interpolation	Second Order Scheme

Spatial Discretization – Momentum	Second Order Upwind
Spatial Discretization – TKE	Second Order Upwind
Spatial Discretization – ω	Second Order Upwind

Table 2 - Summary of Boundary Conditions

Boundary Domain	Boundary Condition
Upper Wall	Wall – Slip (Tangential shear stress=0)
Side Walls	Wall - Slip (Tangential shear stress=0)
Bottom Wall	Wall – No Slip
GAC body	Wall – No Slip
Inlet	Velocity Inlet ($u=15$ m/s, $v=w=0$), Turb Intensity=1%, Turb Viscosity Ratio=10
Outlet	Outflow

5.3 COMPUTATIONAL DOMAIN

The computational domain based on the wind tunnel dimensions of IIT Delhi (where model scale experiments were conducted) is shown in **Figure 3**. The GAC model has been placed in a rectangular domain with sufficient distance to prevent wall effects in the vicinity of the geometry or the glideslope focus region. The inlet has been placed upstream, at a distance of 1L from the GAC body and the outlet has been placed at a distance of 3L

downstream from the aft of GAC, where L is the length of GAC model. The height and width of the domain has been taken as the height and width of the wind tunnel where the in-house experiments were carried out, and are 0.44L (450mm) and 0.733L (750mm) respectively.

error, systematic refinement of space meshes was carried out. For the present study, Grid Convergence studies were carried out for GAC with and without the island structure. The parameters of the Grid Convergence study are shown in **Table 3**. The same parameters are employed for both the studies.

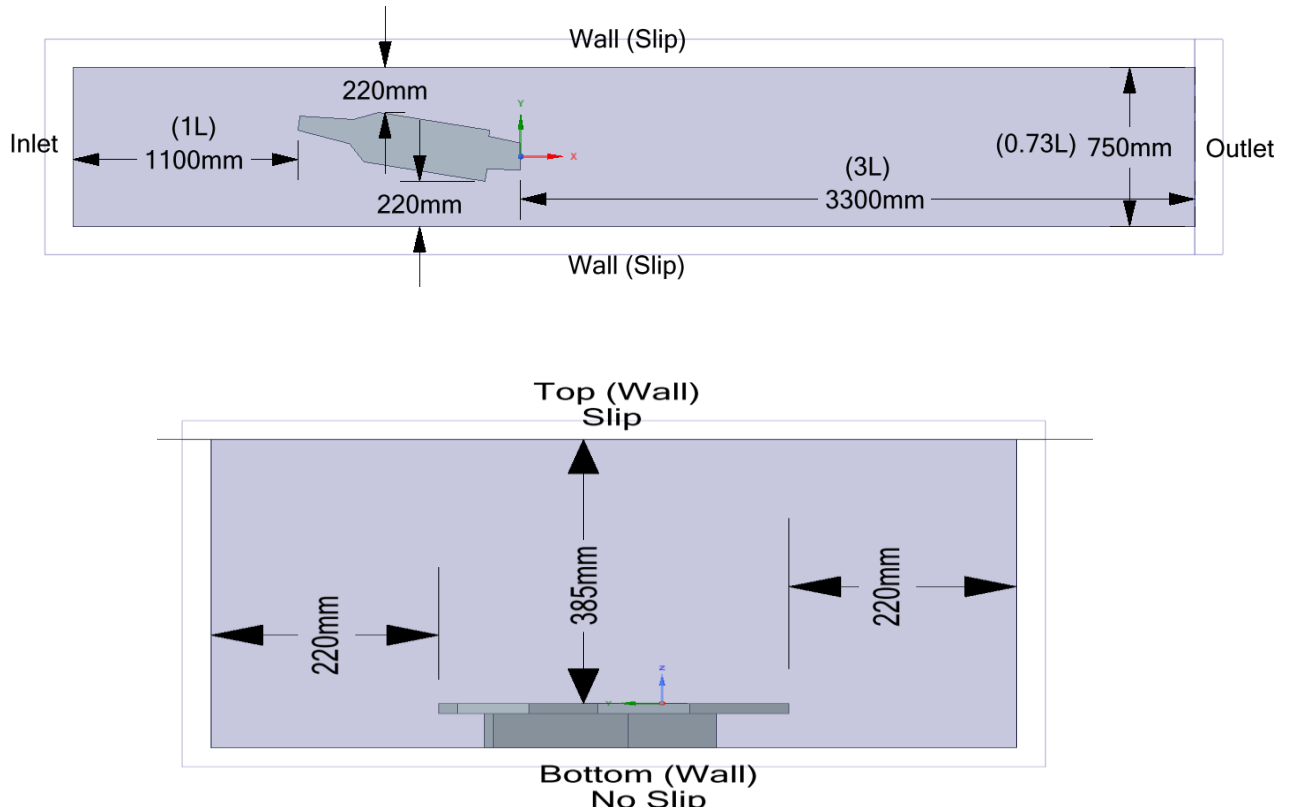


Figure 3:Computational Domain

5.4 SOLVER & MESHING SETUP

Meshing was undertaken in ANSYS Workbench which uses the ICEM CFD as the backend mesher. The GAC being an irregular shaped body, hybrid meshing was carried out using a mixture of tetrahedrons and hexahedrons (Multizone Meshing). Further, since the flight deck of an Aircraft Carrier behaves essentially as a flat plate, capturing the boundary layer growth was of prime importance. To capture the effects of boundary layer, inflation meshing was undertaken by extruding prism layers from the surface body of GAC, to sufficient height to encompass the boundary layer. For $k-\omega$ SST turbulence Model to be effective, y^+ should be ideally less than 1. The number of prismatic layers were chosen as 30, sufficient to encompass the Boundary layer growth. Further, to capture the flow accurately along the body, finer mesh was provided in the vicinity of GAC body using Density Box/ Body of Influence option in the Workbench/ICEM CFD.

In any CFD study, it is important to reduce the round-off, iterative convergence and discretization errors. Round-off error has been minimized by opting for double-precision. The iterative convergence error has been quantified through the truncation criteria for all the residuals, in this case being 10^{-5} . To quantify and reduce the discretization

Table 3- Parameters for Grid Independence Studies

Parameters	Coarse Mesh	Medium Mesh	Fine Mesh
Inflation Details	0.009mm, 30 layers	0.009mm, 30 layers	0.009mm, 30 layers
Face element size on GAC	2.8mm	2.25mm	1.8mm
Element Size close to body (Density Box)	2.8mm	2.25mm	1.8mm
Element Size/Max Size	9.5mm/11.3 mm	7.5mm/9m m	6mm/7.1m m
Total No of Elements	11M cells approx	16M cells approx	22M cells approx

For carrying out the grid independence study, the parameters selected were the normalised u-velocity and

w-velocity along the 3 degree glide slope path. The medium mesh was able to capture accurately the u and w velocities along the burble line and no evident increase in accuracy was obtained by going for the fine mesh (**Figure 4** plots the normalised u & w velocities along 3⁰ glideslope path for all the fine, medium and coarse mesh). Hence, for this study as well as all the parametric studies, the Medium mesh has been adopted. **Figure 5** shows the meshing details using medium mesh for the GAC configuration.

RANS. For the Unsteady RANS, the flow solution was initiated as steady state with 5000 iterations, the unsteady solution was then run with a time step of 0.001 s. The CFD solution requires a settling down time, t_{set} , for repeatable unsteady solution; the settling down time was taken as $t_{set} = \frac{2.5L}{V}$, where L is the characteristic length over which the fluid will pass and V is the free stream velocity (Kelly, M. White, *et al.*, 2016). For the model-scale solution the unsteady flow field was solved for 1.5 s for both the models. The last 0.6 seconds were used for time averaging

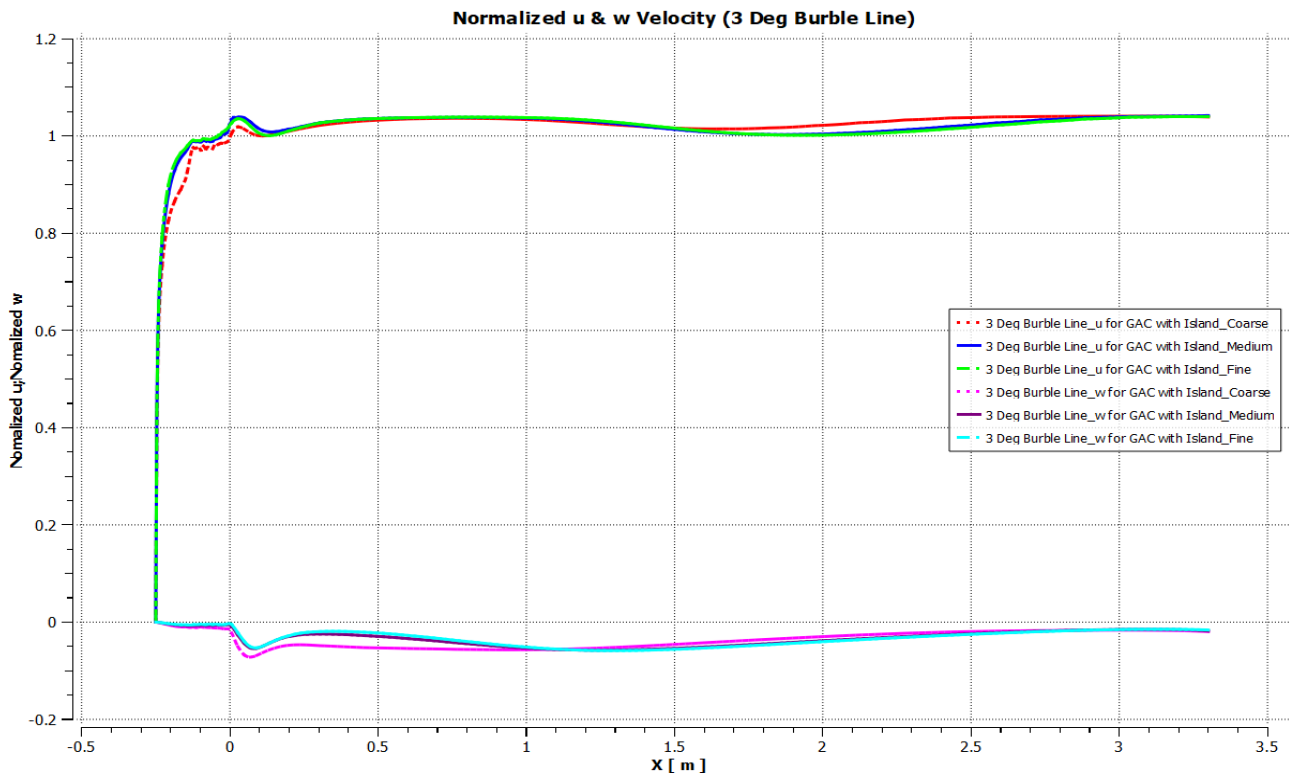


Figure 4: Normalised u & w velocities along 3⁰ glideslope path for the three mesh sizes for GAC

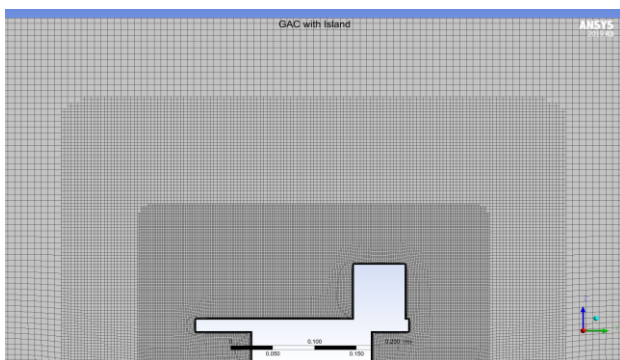


Figure 5: Meshing Details of GAC configuration using Medium mesh

5.5 COMPARISON STEADY AND UNSTEADY RANS

CFD simulations on BGAC and GAC configurations were performed using Steady State RANS and Unsteady

the statistical variables. **Figure 6** compares the steady state Normalised u-velocity and w-velocity with the Normalised time –averaged unsteady u & w velocities along the 3 degree glideslope line for the GAC without island and with island respectively. Also superimposed in this figure, is the instantaneous plot of normalised u & w velocities at t=1.5s. The time-averaged values and the steady state values coincide for both the models and hence the assumption of undertaking steady state analysis for the parametric studies stands justified. For all further studies, the CFD analysis was carried out using the steady state assumption.

6. VALIDATION STUDIES

Prior to carrying out design studies on aircraft carriers through optimization of the aerodynamic wake around the carriers, it is of utmost importance to validate the CFD results with experiments. For the numerical studies discussed hereafter, the numerical CFD results have been validated with in-house data obtained through

experiments, for the 2 extreme hull form configurations, namely GAC with island (GAC) and the GAC without island (BGAC). Further, post validating the numerical results with the optimised turbulence model, qualitative and quantitative comparative analysis have been carried out with published data in open source for aircraft carriers with similar configuration as GAC.

reading scale is magnified by a factor of 2. The resultant uncertainty in the calculated pressure (normalised) is found to be +/- 0.02 (absolute value of Cp).

For validation and choosing the most suitable turbulence model that best represents the physics of this problem, a quantitative analysis was carried out. The local pressure

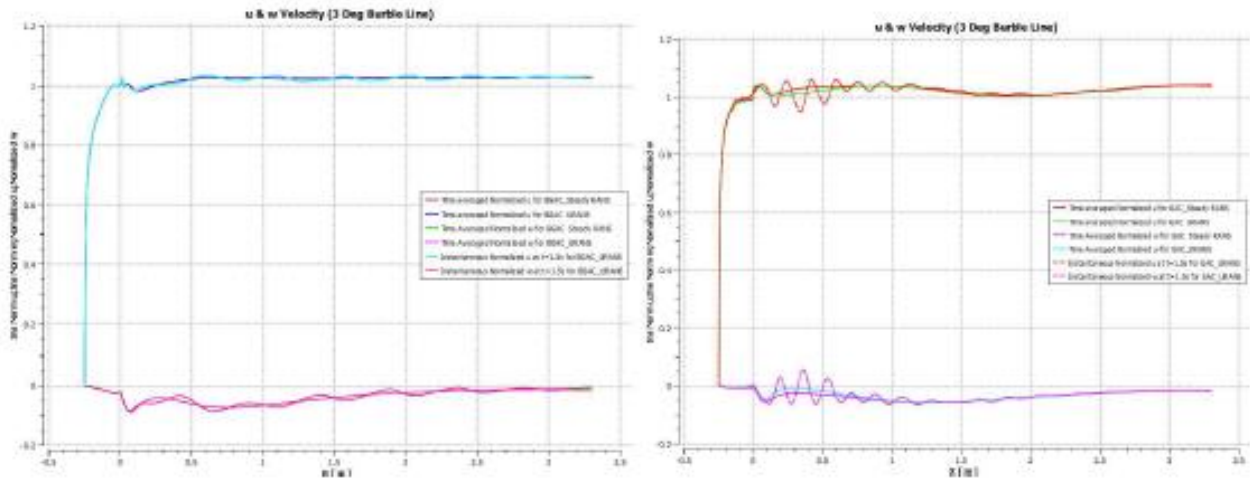


Figure 6: Normalised u & w-velocity (Steady, Unsteady & instantaneous velocities t =1.5s) for BGAC & GAC configurations

6.1 VALIDATION WITH IN-HOUSE EXPERIMENTS

A wooden model of the Generic Aircraft Carrier described in Section 4 and depicted in Figure 3 was fabricated for conducting tests in the wind tunnel. The assembled model consists of three parts, namely, the hull and the flight deck fused together, and a removable island superstructure. The aim of the experiment was to capture the pressure distribution over the deck of the carrier. Towards this objective, a total number of 105 pressure taps were inserted into the flight deck by carefully drilling holes at various locations. The siting of these taps was done to capture data at as many discrete points as possible subjected to the practical restrictions imposed by the fabricated model such as joints, corners, etc. The locations of the pressure taps are shown in Figure 7.

values were extracted from each of the pressure tap locations from the computational model. Pressure coefficient (C_p) at i^{th} pressure tap location, defined as in Equation 3, was calculated at each location.

$$C_{p_i} = \frac{p_i - p_{\infty}}{\frac{1}{2} \rho V^2} \tag{3}$$

This was compared against the pressure coefficients obtained from the corresponding pressure tap in the experiments. A prediction error index E , as defined by Equation 4, was computed to obtain a global measure of agreement that a turbulence model has with the experimental data. It is a measure of the global root mean square error in CFD prediction as compared to the experimental data, expressed as a percentage.

$$E = \frac{1}{N} \sum_{i=1}^N \sqrt{\left(\frac{C_{p_i}(cfD) - C_{p_i}(exp)}{C_{p_i}(exp)} \right)^2} \tag{4}$$

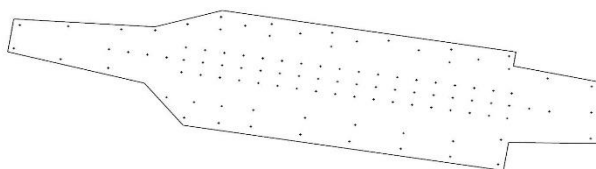


Figure 7: Position of Pressure Taps in GAC Model

The pressure distribution was measured experimentally for both, GAC and BGAC configurations for the pressure point locations as shown in Figure 7. The multitube manometer which was used for the pressure measurements has a least count of 1mm water column. Considering the inclination of 60° that was used for the experiments, the

The exercise was repeated with results obtained from simulations using various turbulence models which were employed for this study. From the analysis, it emerged that the SST k- ω turbulence model shows the best agreement with experimental data with a prediction error of 7.69% in the case of the BGAC configuration and 6.9% in the case of GAC configuration (K Vignesh Kumar *et al.*, 2018). Figures 8 & 9 show the plot of C_p (SST k ω Model vs Experimental Data) along the centreline pressure taps for the BGAC and GAC

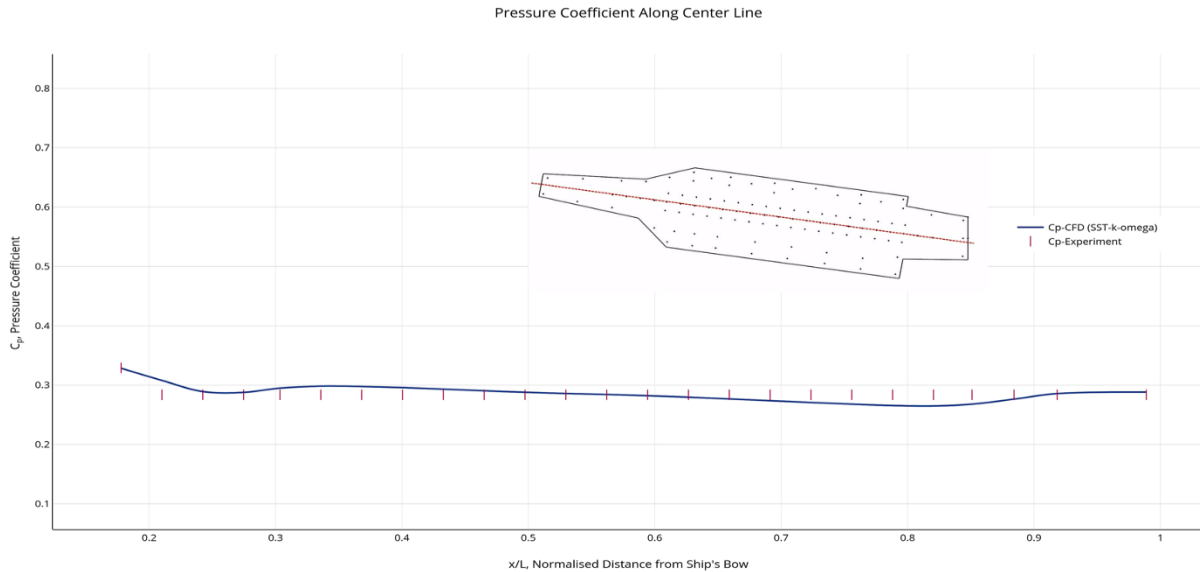


Figure 8: Comparison of Cp along Centre Line – SST $k \omega$ Model vs Expt Data (BGAC)

configurations respectively. Further, PIV measurements to measure velocity and turbulence levels along various transverse planes (YZ plane) behind the GAC (and BGAC) model were carried out and the experimental results were within a range of 6% of the CFD simulations, in the regions of interest (K Vignesh Kumar, 2020).

6.2 VALIDATION WITH PUBLISHED RESULTS IN OPEN DOMAIN

The next set of studies was to validate the CFD results with other experimental results carried out on a representative class of aircraft carriers. There is a dearth of open experimental results, primarily because of the confidentiality of the nature of studies. The most quoted paper in this field is by Cherry and Constantino (Cherry and Constantino, 2010), wherein wind tunnel tests were carried out on a 6 ft long simplified version of the Nimitz

Class carrier, at a Reynolds No. of 11,000,000. Experiments were carried out using a five-hole Pitot probe rake system. Along a vertical plane, located at a distance of $1/3^{rd}$ L aft of the model, the velocity profile and flow angularity were measured. For running the CFD studies, the hull and the flight deck of the GAC model were retained the same as it was very similar to the Nimitz Class. The cuboid model of the superstructure was replaced with the model of the Nimitz and Ford class of superstructures as per the details made available in the paper and other open sources. The contour plots of u-velocity, pitch angle and the yaw angle at a distance of one-third the length of the aircraft carrier models aft of stern of the Nimitz class carrier model, were compared with those of the GAC model fitted with the Nimitz and Ford island structures and good qualitative and quantitative comparison was obtained. **Figure 10** shows the contours of Yaw Angle obtained from Wind Tunnel

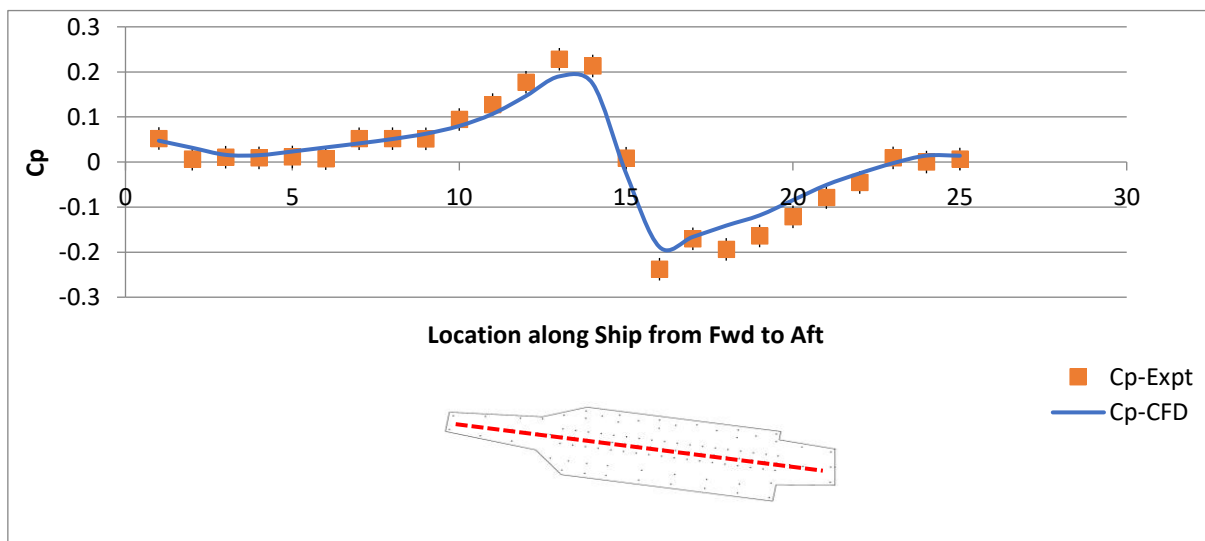


Figure 9: Comparison of Cp along Centre Line – SST $k \omega$ Model vs Expt Data (GAC)

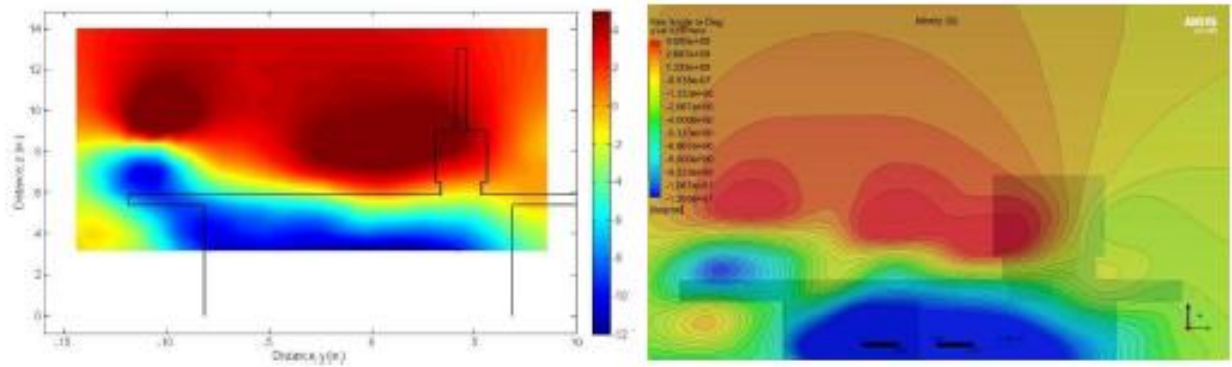


Figure 10: Comparison of Yaw Angles between Wind Tunnel & CFD results (USS Nimitz)

and CFD for Nimitz SS configuration. The forward velocity deficits obtained from the GAC model was in line with the published results.

Further, from the airwake simulation of GAC configuration, the u-velocity along the 3⁰ glideslope path was plotted and compared with the MILSPEC burble ('MIL-F-8785C: Flying Qualities of Piloted Airplanes', 1980). There was good general agreement for the 3⁰ glideslope path and the velocity 'dip' between 1.4-2 ship lengths was captured ('MIL-F-8785C: Flying Qualities of Piloted Airplanes', 1980) (Kelly *et al.*, 2018).

7. QUANTIFYING PILOT WORKLOAD AND BURBLE EFFECT

Prior to undertaking parametric studies, it is essential to have a mathematical model for quantifying the pilot workload and the effect of the burble, as a function of flow/airwake characteristics without bring in the pilot into the simulation loop. Pilot workload is a subjective term and there is still no generally accepted definition. Miller and Hart (Miller and Hart, 1984) has identified nine dimensions which effect total workload: task difficulty, time pressure, own performance, mental effort, physical effort, frustration, stress, fatigue, and activity type. The Cooper-Harper Handling Qualities Rating Scale (HQRS) (Cooper and Harper, 1969) (Harper and Cooper, 1986), is a pilot rating scale, which is used to evaluate aircraft handling qualities based on a set of criteria. The scale has a range of 1 to 10, with 1 indicating the best and 10 the worst aircraft handling qualities. However the rating is subjective. There are other indices being used such as NASA Task Load Index (NASA TLX) etc. These indices still depend on the subjective opinion of a pilot actually flying the missions. These indices give a quantitative indication of the aircraft handling qualities and are more appropriate for specific aircraft being operated by pilots. From a Naval Ship Designer's perspective, the flow/airwake characteristics of ship along a specified glide path, which impact the pilot's workload is more appropriate. As per studies undertaken by Rudowsky *et al.*, (Rudowsky *et al.*, 2002), any decrease in forward velocity component (u) would be considered unfavourable

for pilot workload and safety, as it directly reduces the lift force and causes a sinking effect. The research study conducted by Vivaldi (Vivaldi, 2004), analysed the effect of turbulence and crosswinds on mental workload of pilots. The study concluded that turbulence, and in specific, turbulence intensity, was the major contributor to pilot workload. The study used simulators and on-board measurements to measure air speed fluctuations and other parameters across a range of test pilots. The Turbulent Kinetic Energy (TKE) or the Turbulent Intensity (TI), along the specified glideslope path, would give a quantitative indication of the disturbance faced by the pilot and could be used as one of the measures of quantifying burble. Average Turbulent Kinetic Energy along the glideslope, is the integral of the TKE along the glideslope line divided by the length of the glideslope line and is thus mathematically given by the equation:

$$TKE_{Average} = \frac{\oint TKE dl}{\oint dl} = \frac{\oint TKE dl}{l} \quad (5)$$

Further, an aircraft approaching a carrier is already on the verge of stall because of low speed and high angle of attack, and when it approaches the velocity deficit burble region, the lift on the wing further decreases causing the aircraft to sink (Cherry and Constantino, 2010). Thus any decrease in the velocity compared to the far-stream velocity would add on to the 'burble effect' and this average variation in the u-velocity, $u_{Av_Variation}$, along the designated glideslope path, can be mathematically quantified as:

$$u_{Av_Variation} = \frac{\oint \oint |Abs(u - U_{far stream})| dl}{\oint \oint |Abs(u - U_{far stream})| dl} = \frac{\oint \oint |Abs(u - U_{far stream})| dl}{l} \quad (6)$$

In addition, the aircraft also flies through a region where the flow has a downwash, typically between 1-2 m/s (Gaddis, 2009). This region of downward flow coincides with the region of lower flow velocity caused by the aircraft carrier and therefore adds on to the "burble effect". This downwash, $w_{Av_Variation}$, along the designated glideslope path, can be mathematically quantified as:

$$w_{Av_Variation} = \frac{\oint \oint |Abs(w)| dl}{\oint \oint |Abs(w)| dl} = \frac{\oint \oint |Abs(w)| dl}{l} \quad (7)$$

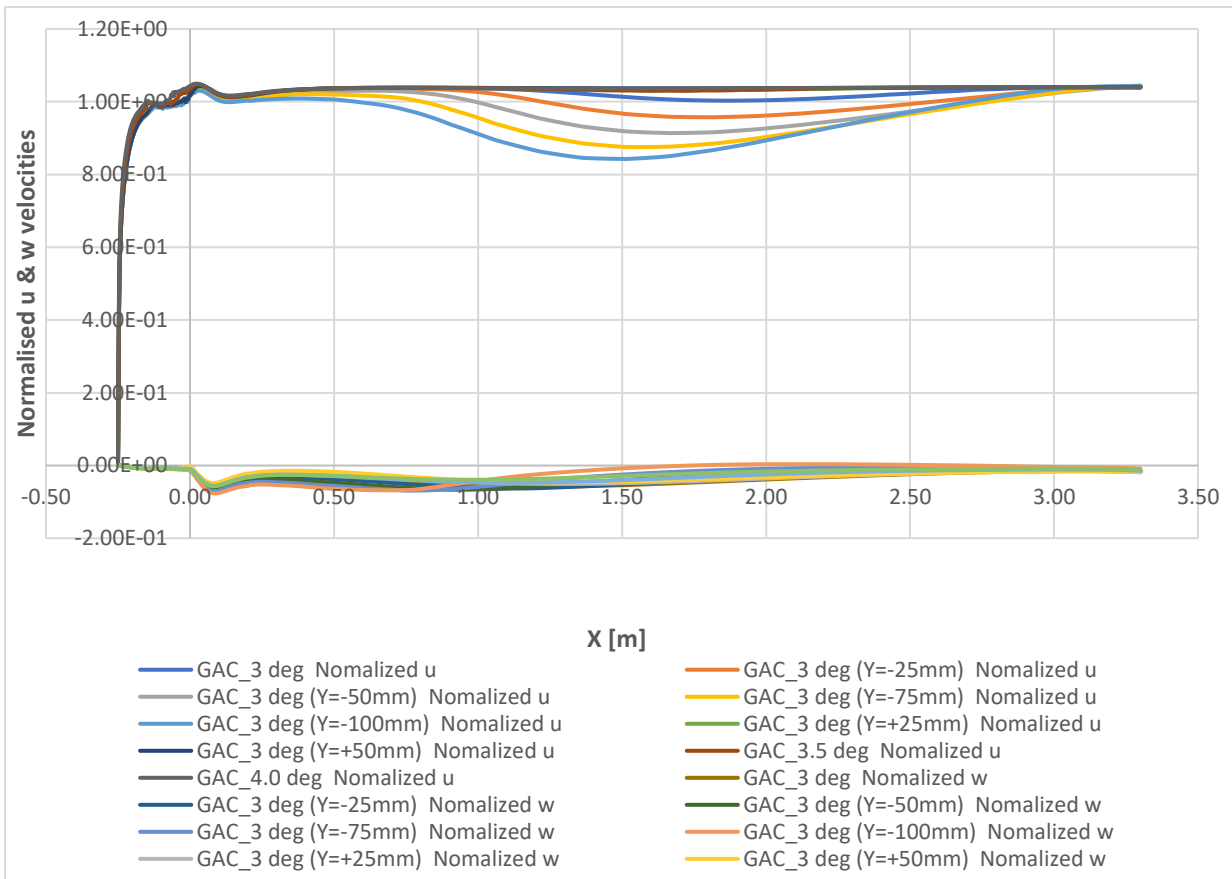


Figure 11: Normalised u & w velocities along different Glide slope path (GAC)

Together, $TKE_{average}$, $u_{Av-Variation}$ and $w_{Av-Variation}$, would give a quantitative estimate of the burble produced by different parametric changes and also a quantitative indication of the potential pilot workload because of the physical flow features in the airwake of an aircraft carrier. However, here it is pertinent to mention that these mathematical constructs needs to be correlated with piloted flight simulations.

8. RESULTS AND DISCUSSION

The results have been presented as line plots and contour plots of velocity and pressure. The line plots have been plotted along the various glideslope paths for u, w and Turbulence Kinetic Energy (TKE). The glide slope (or glide path) is an imaginary line that gives the trajectory of the aircraft flight till its landing at the Touch Down Point(TDP) on an aircraft carrier. The 3 degree glide slope path is the usual and preferred approach path for the aircraft landing on an aircraft carrier. The 3.5° and the 4° glide slope paths have also been studied as certain navies operate at these glideslope paths. The other glideslope path are derived from the 3° approach path by laterally deviating by 100mm (yawed by 1.61°), 75 mm (yawed by 1.21°), 50mm (yawed by 0.80°) and 25 mm (yawed by 0.40°) towards the starboard and 50mm (yawed by 0.80°) and 25mm (yawed by 0.40°) towards port from the approach end (i.e. at a distance of

3300mm in model scale from the stern of the carrier), resulting in a total of 7 paths for 3° approach. The yawed glide paths take into effect the pilot’s navigational error from the 3° glidepath. Results of the CFD simulations are presented in the following paragraphs.

8.1 COMPARATIVE STUDY OF GAC & BGAC CONFIGURATIONS

The plots of the u-velocity, w-velocity and TKE along various glideslope paths as well as the velocity contour plots along the transverse planes have been used for carrying out a comparative study of GAC and BGAC configurations.

8.1 (a) u & w VELOCITY PROFILES ALONG VARIOUS GLIDESLOPE PATHS

Figure 11 shows the u & w-velocity plots respectively for various glideslope paths namely 3° , 3.5°, 4° and 3° glideslope path laterally shifted by -25mm, -50mm, -75mm, -100mm, +25mm & +50mm for GAC configuration. The – sign indicates a lateral shift to the port and +ive indicates lateral shift to starboard.

It can be seen from Figure 11 that the u-component of the flow (normalised by far-stream velocity) offers good general agreement for the 3° glideslope, capturing the velocity “dip” between 1.4 - 2 ship lengths, which the

MILSPEC burble also predicts. Further, there is a continuous dip in u-velocity from 0.5L aft of the stern. Figure 11 also shows that there is a slight downwash along the approach path, which gets aggravated as a ‘dip’ very close to the stern. Thus it can be concluded that even for a small island structure, modelled as a cuboid, which is already highly optimised, the evidence of a burble is very clear and the GAC model is able to capture it. It can be very well argued, that had the island been a little more bulkier, the burble would have been more pre-dominant and could have replicated the ‘MILSPEC’ burble, which was based on pilot studies carried out on aircraft carriers in the late 1960s, with much bulkier island structures (Specification, 1980). By analysing the flows for steeper glideslope path of 3.5° and 4°, it was seen that the dip in u-velocity seen between 1.0-2.5 ship lengths was not visible for the 4° glideslope path and was negligible for the 3.5° path. However, all the three glideslope paths show a continuous dip in u-velocity from 0.5L aft of stern. This suggests that the disturbances to the flow because of the island and the flight deck configuration, occurs at a lesser height as compared to the steeper glideslope path of 3.5° and 4° and these disturbances do not interact with the approach path. Coming to the glideslope paths, which were laterally shifted from the 3° glideslope path, it was seen, from Figure 9, that the u-velocity deficit seen between 1.0-2.5 ship lengths was highly predominant in the case of the 100mm yawed path and decreases as the lateral distance moves from port to starboard, being almost negligible for the 25mm (stbd shift) . The forward u-velocity deficit, in the case of 100mm (port shift) was nearly 18%. The differences in the u-velocity deficits between the various glide paths could be attributed to the interaction with regions of greater turbulences, primarily generated by the notches on the port side, as the glideslope path is yawed towards the port. This interaction is manifested as velocity deficits.

Figure 12 shows a comparison of normalised u-velocities between GAC & BGAC configurations for the 3°, 4° and 3°(Y=-100mm) glideslope paths. It is seen that there is no perceptible dip in u-velocity till around 0.5L, for BGAC, unlike in the case of GAC where there is a prominent velocity deficit between 1.4L and 2.5L. It is also seen that in the case of 3°(Y=-100mm) glideslope path, both the configurations show deficit in the u-velocity, but it is more prominent in the case of GAC with island. In the case of GAC, the maximum u-velocity deficit (around the region between 1.4L and 2.5L) is approximately 5% compared to the free-stream velocity, which increases to 18% when the glideslope path is shifted towards port by 100mm. In the case of BGAC, there was no perceptible u-velocity deficit along the 3 degree glideslope path, but when the glideslope path was yawed by 100mm to port, the maximum u-velocity deficit was approximately around 11%. The absence of u-velocity deficit along the 3 degree glideslope path for the BGAC configuration, indicates that a major cause of the u-velocity deficit is the island structure for the case of a GAC. However, as the glideslope path was yawed towards the port, the contribution of the geometrical features like the flight deck notches, sharp features in the bow and the hull itself, play a more prominent role in causing the u-velocity deficit. Thus, u-velocity deficit exists even in the absence of the island (BGAC configuration), for the 3°(Y=-100mm) glideslope path.

Further, an analysis of the down wash velocities (w-velocity) showed that the magnitude of downwash was of the same order for all the yawed paths. However, the onset of downwash differs along different glideslope paths. In the case of 100mm (port shift), the onset of downwash happens closest compared to other paths, at 0.75L from the stern and continues to increase, before a further ‘dip’ near the stern. Onset of downwash closer to the stern, would increase the pilot workload as he has lesser time to

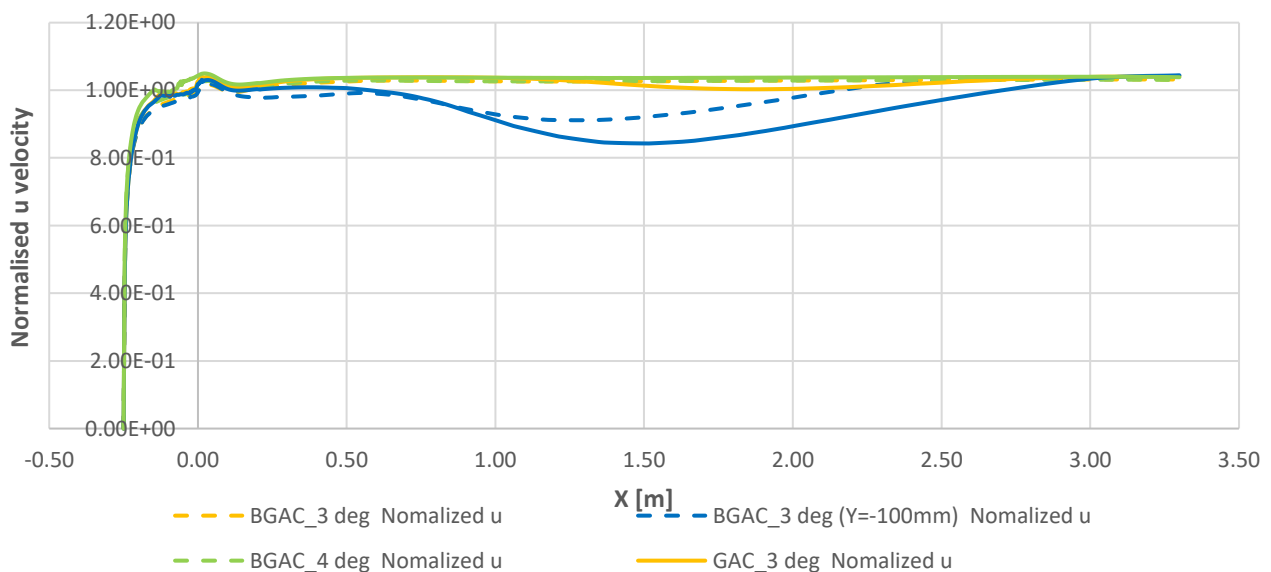


Figure 12: Comparison of u velocities along different glideslope path (GAC vs BGAC)

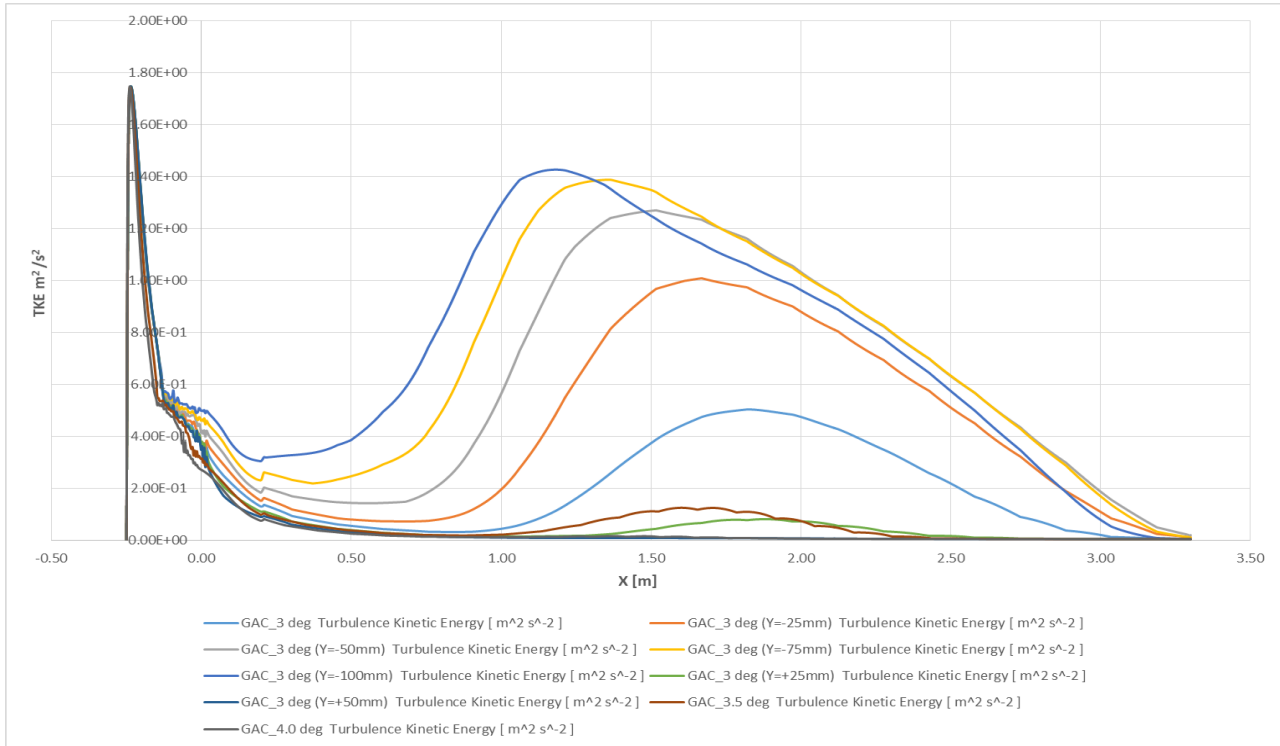


Figure 13: TKE along different glideslope paths (GAC)

take corrective action. A similar trend was seen for the GAC configuration too.

The values of $u_{Av, Variation}$ as defined by Eqn (7) and $\Delta u_{Av, Variation}$ are tabulated below. It can thus be concluded, that as the glideslope path is yawed towards starboard and also, as the angle of approach becomes steeper, the velocity deficit areas through which the glide path passes becomes considerably lesser and could result in reduction of pilot workload.

Table 4 : $u_{Av, Variation}$ & Max u deficit (BGAC vs GAC)

Glideslope	$u_{Av, Variation}$ BGAC	$u_{Av, Variation}$ GAC	$\Delta u_{Av, Variation}$
3 ⁰ glideslope	0.355 m/s	0.204 m/s	0.151 m/s
3.5 ⁰ glideslope	0.286 m/s	0.177 m/s	0.109 m/s
4 ⁰ glideslope	0.275 m/s	0.161 m/s	0.114 m/s
3 ⁰ (100mm Port shift)	1.441 m/s	0.857 m/s	0.584 m/s
3 ⁰ (75mm Port shift)	1.246 m/s	0.635 m/s	0.611 m/s
3 ⁰ (50mm Port shift)	0.971 m/s	0.411 m/s	0.560 m/s
3 ⁰ (25mm Port shift)	0.662 m/s	0.256 m/s	0.406 m/s
3 ⁰ (50mm Stbd shift)	0.210 m/s	0.192 m/s	0.018 m/s

8.2 (b) TURBULENCE KINETIC ENERGY (TKE)

TKE is obtained as the trace of the Reynolds Stress Tensor and is defined as:

$$TKE = \frac{1}{2} \overline{u'_i u'_i} \tag{8}$$

Figure 13 shows the plot of TKE along the 3⁰, 3.5⁰ & 4⁰ and along 3⁰ laterally shifted glideslope paths, for the GAC configuration.

It is seen that the 3⁰ glideslope path has larger TKE throughout the approach path as compared to either the 3.5⁰ and 4⁰ glideslope path. As the glide slope becomes steeper, the TKE along the approach path decreases, because the disturbances caused by the island and the flight deck configurations are at a lower height, as was discussed in the previous section. Further, as can be seen from the figure, the TKE increases, with the maximum TKE being along the 3⁰(Y=-100mm) glideslope path as the glideslope path shifts laterally to the port. This is because as the glide path shifts to the port, it encounters disturbances from the port notches along its glide path, which increases as one travels further port. Further, it is seen that the peak value of TKE shifts closer to the Touch Down Point (TDP), as the glide path shifts laterally to the port. This would be a cause of higher pilot workload, as the pilot would have lesser time for taking correcting actions to offset the disturbances on the aircraft because of the peak TKE. The BGAC configuration shows similar trend in TKE variation along the various glide paths, and will not be further discussed here.

Figure 14 compares the TKE along 3⁰ and 3⁰(Y=-100mm) glideslope path for both the GAC and the BGAC configurations.

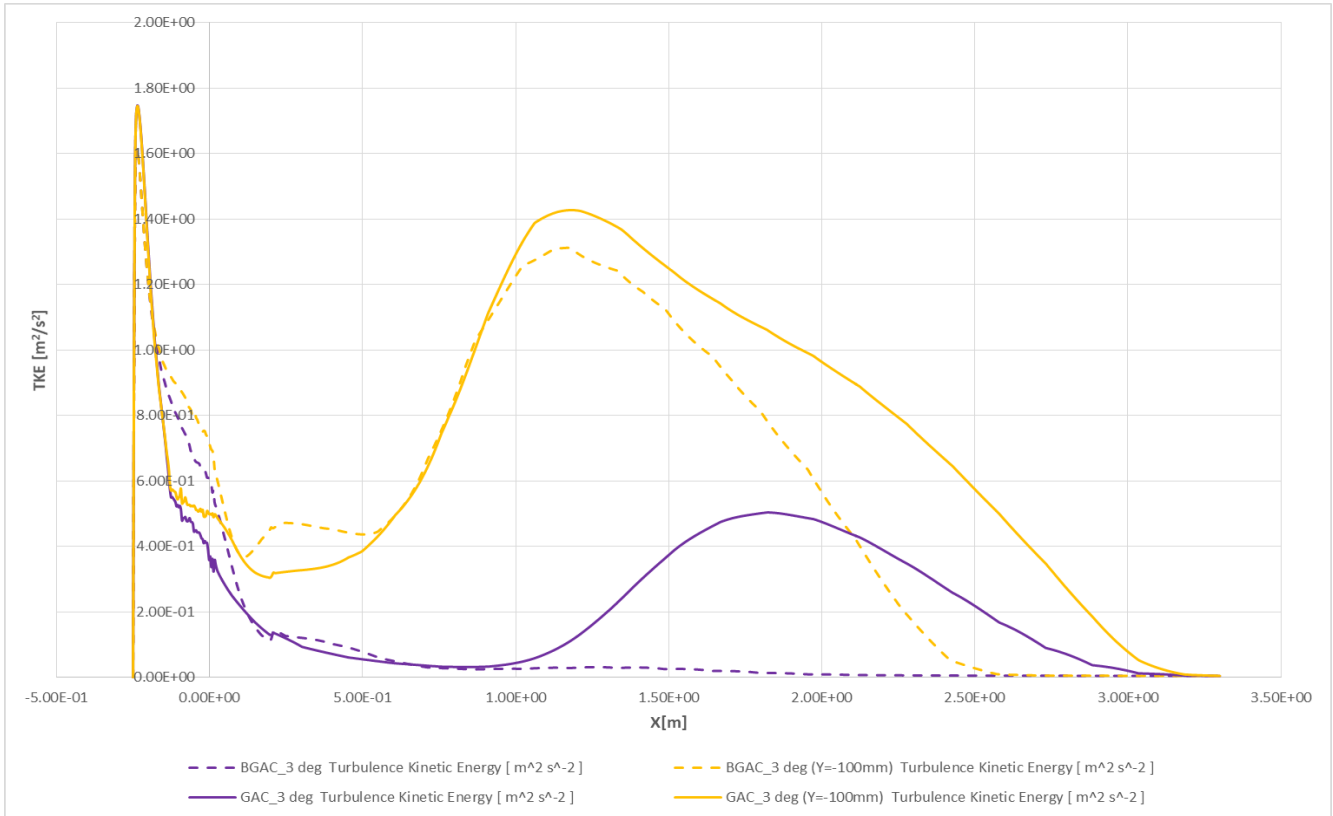


Figure 14: Comparison of TKE (BGAC vs GAC)

As can be seen, the TKE along the 3⁰ glide path up till 0.5L aft of the carrier, is negligible in the case of the BGAC configuration as compared to the GAC configuration. There is no hump (maxima TKE), as is seen for the case of GAC. Thus we can surmise that for 3⁰, 3.5⁰ & 4⁰ glideslope paths, the turbulence is generated by the island structure. However, when the glideslope path is shifted laterally by 100mm to the port [3⁰(Y=-100mm)], both the GAC as well as the BGAC configuration show large TKE along the approach path. Though, for the case of the BGAC variant, the TKE is lesser as compared to the GAC variant, the difference is not as drastic as was the case for the 3⁰ glideslope path. The plots of TKE for GAC and BGAC variants are reasonably close, indicating that along this glideslope path, the turbulence encountered is primarily from the vortices generated at the flight deck notches and the turbulence generated because of the island is not very predominant along this path. It can be surmised, that as the glideslope path is shifted further port, the turbulence encountered would be solely because of the flight deck and hull configuration, with the role of turbulence generated by the island, being very minimal.

The **TKE_{Average}**, have been computed and tabulated in Table 5 for the different glideslope paths for both the GAC and BGAC configurations along with the % change of **TKE_{Average}** of GAC as compared to BGAC.

Table 5 : TKE_{Average} along different glideslope paths (BGAC vs GAC)

Glideslope	TKE _{Average} (BGAC)	TKE _{Average} (GAC)	% change in TKE _{Average}
3 ⁰ glideslope	0.104 J/Kg	0.238 J/Kg	56.3%
3.5 ⁰ glideslope	0.090 J/Kg	0.100 J/Kg	10%
4 ⁰ glideslope	0.082 J/Kg	0.068 J/Kg	-20.5%
3 ⁰ (100mm Port shift)	0.575 J/Kg	0.724 J/Kg	20.5%
3 ⁰ (75mm Port shift)	0.456 J/Kg	0.699J/Kg	34.8%
3 ⁰ (50mm Port shift)	0.291 J/Kg	0.620 J/Kg	53.0%
3 ⁰ (25mm Port shift)	0.154 J/Kg	0.461 J/Kg	66.5%
3 ⁰ (25mm Stbd shift)	0.093 J/Kg	0.096 J/Kg	3.1%
3 ⁰ (50mm Stbd shift)	0.089J /Kg	0.077J /Kg	-15.5%

It is seen, that there is a decrease in turbulence for the BGAC configuration for all glideslope paths, except for the steep 4⁰ glideslope path, for which the TKE for both the configurations is minimal. The decrease in the TKE is approximately 56% along the 3⁰-glideslope path and 20% along the 3⁰(Y=-100mm) glideslope path, indicating that along the 3⁰(Y=-100mm) glideslope path, the disturbances are primarily, because of the flight deck configuration and

the disturbances because of the island are minimal along this glide path.

9. CONCLUSIONS

Two variants of Generic Aircraft Carrier, GAC and BGAC (GAC without island) have been developed as a part of this study, which could serve the purposes of a simplified model of an Aircraft Carrier, for undertaking external aerodynamic studies using various experimental means and validating CFD codes. CFD studies have been carried out on both the variants, using commercially available CFD software ANSYS Fluent. An in-depth study of the airwake around the GAC has been carried out. The features responsible for the generation of turbulence are the island structure and the notches on the flight deck and the sharp bow edge. In the absence of the island, the flight deck notches are a primary contributor to the generation of turbulent structures. The studies have shown, that even in the case of the GAC, which has a highly optimised and volumetrically small island structure (the area occupied by the island being less than 5% of the total flight deck area), the 'burble effect' behind the carrier, was very much present, and in case of larger islands, there would have been greater resemblance to the MILSPEC burble.

It was seen that there is a decrease of 56% in $TKE_{average}$ for the BGAC variant as compared to the GAC variant, along the 3 degree glideslope. Thus along the 3-degree glideslope, the turbulence was primarily generated because of the presence of the island which is a blunt body. However, as the glideslope was yawed towards starboard by 100mm, along the same 3 degree angle [$3^0(Y=-100mm)$], the decrease in $TKE_{average}$ for BGAC variant compared to GAC was only 20%, which shows that along the yawed glideslope path, the turbulence was primarily because of the configuration of the flight deck, especially the port notches.

A similar analysis of the maximum deficit in forward velocity (u-velocity) along the glideslope paths showed that between 0.5L and 2L aft of stern, the deficit in u-velocity for GAC configuration was 5% for the 3^0 glideslope path and 18% for $3^0(-100mm)$ glideslope path and for BGAC, the deficit in u-velocity was negligible for the 3^0 glideslope path and was 11% for $3^0(-100mm)$ glideslope path.

The average downwash and the maximum downwash for 3^0 glideslope path for GAC and BGAC were nearly the same and was approximately between 4-6% of the free stream velocity. The downwash was more dependent on the flight deck and Hull configuration and the presence of the island in attenuating the downwash was negligible.

Thus, it can be concluded from the CFD studies undertaken, that in the case of a typical Aircraft Carrier, where the island structure has been completely eliminated, the turbulence along the 3^0 glideslope path (mathematically modelled as TKE) comes down

drastically. There is also 5-8% reduction in the deficit in the forward velocity. However in both the configurations (with and without island), the average downwash is in the range of 4-5% of free-stream velocity and is always present along the 3^0 glideslope path. Further, as the glideslope paths are shifted laterally towards starboard, or the approach angle is increased from 3 degree, the areas of turbulence intersecting the glideslope paths become lesser and lesser, and consequently there could be a resultant decrease in the pilot workload.

10. REFERENCES

1. BARDERA-MORA, R., BARCALA-MONTEJANO, M. A., RODRÍGUEZ-SEVILLANO, A. and NOVA-TRIGUEROS, J. (2016) 'Passive flow control over the ski-jump of aircraft carriers', Ocean Engineering, 114, pp. 134–141. doi: 10.1016/j.oceaneng.2016.01.019.
2. BARDERA-MORA, R., RODRÍGUEZ-SEVILLANO, A., LEÓN-CALERO, M. and NOVA-TRIGUEROS, J. (2018) 'Three-dimensional characterization of passive flow control devices over an aircraft carrier ski-jump ramp', Proceedings of the Institution of Mechanical Engineers, Part G: Journal of Aerospace Engineering, 232(15), pp. 2737–2744. doi: 10.1177/0954410017716195.
3. BARDERA-MORA, R., LEÓN CALERO, M. and GARCÍA-MAGARIÑO, A. (2018) 'Aerodynamic effect of the aircraft carrier island on flight deck flow with cross wind', Proceedings of the Institution of Mechanical Engineers Part M: Journal of Engineering for the Maritime Environment, 232(2), pp. 145–154. doi: 10.1177/1475090216689172.
4. BARNETT, W. F. and WHITE, H. E. (1963) 'Comparison of the Airflow Characteristics of Several Aircraft Carriers', Oceanics, Report No 64-16, Office of Naval Research, Dept of the Navy, Washington D.C 20360.
5. CHERRY, B. E. and CONSTANTINO, M. M. (2010) 'The Burble Effect - Superstructure and Flight Deck Effects on Carrier Air Wake', in American Society of Naval Engineers Launch & Recovery Symposium. Annapolis: Available at: <https://apps.dtic.mil/sti/pdfs/ADA527798.pdf>.
6. COOPER, G. E. and HARPER, R. P. (1969) *The use of pilot rating in the evaluation of Aircraft Handling Qualities*, NASA Technical Note NASA-TN-D-5153.
7. CZERWIEC, R. M. and POLSKY, S. A. (2004) 'LHA airwake wind tunnel and CFD comparison with and without bow flap', Collection of Technical Papers - AIAA Applied Aerodynamics Conference, 1, pp. 207–214. doi: 10.2514/6.2004-4832.
8. DURAND, T. and TEPER, G. (1964) 'An Analysis of Terminal Flight Path Control in

- Carrier Landing', Systems Technology Inc, 137(1).
9. FRAUNDORF, M. (1966) 'Investigation of means of reducing aircraft Carrier turbulence', Dynasciences Corporation, Blue Bell, Pennsylvania;
 10. FROST, S. (1968) 'Aircraft Carrier Turbulence Study for Predicting Air Flow Dynamics with Increasing Wind Over Deck Velocities', National Technical Information Service, US Naval Air Engineering Center.
 11. GADDIS, D. E. (2009) *NATOPS- Landing Signal Officer Manual*. Available at: <https://info.publicintelligence.net/LSO-NATOPS-MAY09.pdf> (Accessed: 14 October 2017).
 12. HARPER, R. P. and COOPER, G. E. (1986) 'Handling qualities and pilot evaluation', *Journal of Guidance, Control, and Dynamics*, 9(5), pp. 515–529. doi: 10.2514/3.20142.
 13. K VIGNESH KUMAR, MATHEW, M., SINGH, S., SINHA, S. S. and VIJAYAKUMAR, R. (2018) 'Experimental investigation of flow over the flight deck of a Generic Aircraft Carrier', in *Warship 2018- Procurement of Future Surface Vessels*. London, UK: Royal Institute of Naval Architects, UK.
 14. K VIGNESH KUMAR (2020) *Some flow studies on the effect of the island on the flight approach path of a generic aircraft carrier*. Phd Thesis: Indian Institute of Technology, Delhi.
 15. KELLY, M. F., WHITE, M. D., OWEN, I. and HODGE, S. J. (2016) 'The Queen Elizabeth Class Aircraft Carriers : Airwake Modelling and Validation for ASTOVL Flight Simulation The Queen Elizabeth Class Aircraft Carriers : Airwake Modelling and Validation for ASTOVL Flight Simulation', in *ASNE Launch and Recovery Symposium 2016*. Maryland, USA: American Society of Naval Engineers.
 16. KELLY, M. F., WATSON, N. A., HODGE, S. J., WHITE, M. D. and OWEN, I. (2018) 'The Role of Modelling and Simulation in the Preparations for Flight Trials Aboard the Queen Elizabeth Class Aircraft Carriers', *Proceedings of the International Naval Engineering Conference and Exhibition (INEC)*, 14(October), pp. 1–16. doi: 10.24868/issn.2515-818x.2018.037.
 17. KELLY, M. F., WHITE, M. and OWEN, I. (2016) 'Using airwake simulation to inform flight trials for the Queen Elizabeth Class Carrier', in *13th International Naval Engineering Conference*. Bristol, UK.
 18. LANDMAN, D., LAMAR, J. E. and SWIFT, R. (2005) 'Particle Image Velocimetry Measurements to Evaluate the Effectiveness of Deck-Edge Columnar Vortex Generators on Aircraft Carriers', *NATO AVT Conference*, pp. 1–16.
 19. LEHMAN, A. F. (1966) 'An experimental study of the dynamic and steady-state flow disturbances encountered by aircraft during a carrier landing approach', *Journal of Aircraft*, 3(3), pp. 208–212. doi: 10.2514/3.43726.
 20. MENTER, F. R. (1994) 'Two-equation eddy-viscosity turbulence models for engineering applications', *AIAA Journal*, 32(8), pp. 1598–1605. doi: 10.2514/3.12149.
 21. 'MIL-F-8785C: Flying Qualities of Piloted Airplanes' (1980), pp. 1–94.
 22. MILLER, R. C. and HART, S. G. (1984) 'Assessing the Subjective Workload of Directional Orientation Tasks', in *20th Annual Conference on Manual Control*.
 23. NANGIA, R. . and LUMSDEN, R. . (2004) 'Novel vortex flow devices - columnar vortex generators studies for airwakes', *34th AIAA Fluid Dynamics Conference*, pp. 1–18. doi: 10.2514/6.2004-2348.
 24. OWEN, I., LEE, R., WALL, A. and FERNANDEZ, N. (2021) 'The NATO generic destroyer – a shared geometry for collaborative research into modelling and simulation of shipboard helicopter launch and recovery', *Ocean Engineering*, 228(April). doi: 10.1016/j.oceaneng.2020.108428.
 25. POLSKY, S. A. and BRUNER, C. (2002) 'A computational study of unsteady ship airwake', *AIAA Aerospace Sciences Meeting and Exhibit*, 40(1), p. 1022. doi: 10.2514/6.2002-1022.
 26. POLSKY, S. and NAYLOR, S. (2005) 'CVN airwake modeling and integration: Initial steps in the creation and implementation of a virtual burble for F-18 carrier landing simulations', *Collection of Technical Papers - AIAA Modeling and Simulation Technologies Conference 2005*, 2, pp. 797–805. doi: 10.2514/6.2005-6298.
 27. RINGLEB, F. . (1963) 'Three Dimensional Smoke Tunnel Studies of Wind Over Deck of Aircraft Carriers', in *Naval Air Engineering Laboratory(NAEL) Report NAEL-ENG-7019*.
 28. RUDOWSKY, T., HYNES, M., LUTHER, M. and SENN, P. (2002) *Review of the Carrier Approach Criteria for Carrier-Based Aircraft*, Technical Report, Naval Air Warfare Center Aircraft Division. U.S. Navy.
 29. SHIPMAN, J., ARUNAJATESAN, S., MENCHINI, C. and SINHA, N. (2005) 'Ship airwake sensitivities to modeling parameters', *43rd AIAA Aerospace Sciences Meeting and Exhibit - Meeting Papers*. doi: 10.2514/6.2005-1105.
 30. SHIPMAN, J. D., ARUNAJATESAN, S., CAVALLO, P. A., SINHA, N. and POLSKY, S. A. (2008) 'Dynamic CFD simulation of aircraft recovery to an aircraft carrier', *Collection of Technical Papers - AIAA Applied Aerodynamics Conference*, (August), pp. 1–11. doi: 10.2514/6.2008-6227.
 31. SMITH, D. V. (2010) *One Hundred years of US Navy Air power*. US Naval Institute Press.

32. Specification, MILITARY. (1980) *MIL-F-8785C: Flying Qualities of Piloted Airplanes*, United States Department of Defense.
33. VIVALDI, B. E. (2004) '*The Effect of Crosswind and Turbulence in Mental Workload and Pilot Tracking Performance Embry-Riddle Aeronautical University*', MS Thesis - Embry-Riddle Aeronautical University, Daytona Beach, Florida.
34. WATSON, N. A., KELLY, M. F., OWEN, I., HODGE, S. J. and WHITE, M. D. (2019) '*Computational and experimental modelling study of the unsteady airflow over the aircraft carrier HMS Queen Elizabeth*', *Ocean Engineering*, 172(December 2018), pp. 562–574. doi: 10.1016/j.oceaneng.2018.12.024.